

Comment on the manuscript 1806.02080v1 entitled “Spurious finite-size instabilities of a new Gogny interaction suitable for astrophysical applications”

C. Gonzalez-Boquera, M. Centelles, X. Viñas

Departament de Física Quàntica i Astrofísica and Institut de Ciències del Cosmos (ICCUB),
Facultat de Física, Universitat de Barcelona, Martí i Franquès 1, E-08028 Barcelona, Spain

L.M. Robledo

Departamento de Física Teórica, Facultad de Física, Universidad Autónoma de Madrid,
E-28049 Madrid, and Center for Computational Simulation, Universidad Politécnica de Madrid,
Campus de Montegancedo, Boadilla del Monte, E-28660 Madrid, Spain

Abstract

The conclusions of the manuscript 1806.02080v1 questioning the adequacy of the recently proposed Gogny D1M* interaction for finite nuclei calculations using harmonic oscillator (HO) basis are revised. Several convergence and stability studies are performed with HO basis of different sizes and oscillator parameters and the results show the robustness of the D1M* results for finite nuclei. This analysis is also extended to beyond mean-field calculations of generator-coordinate-method type with D1M*. On the other hand, the existence of a finite-size instability in finite nuclei when coordinate space methods are used to solve the HF equations (as shown in 1806.02080v1) is independently confirmed for D1M* using an in-house computer code based on a quasilocal approximation to the HF exchange potential. We confirm that the most affected quantity in the coordinate space calculation is the spatial density at the origin, but integrated quantities like binding energies or radii show a plateau against the number of iterations, where they are consistent with the values from the HO basis calculation, before diverging for a larger number of iterations. A connection between the last occupied s -orbital in the nucleus and the appearance of instabilities in coordinate space is observed.

In Ref. [1] we proposed a new parametrization D1M* of the Gogny interaction, aimed to predict a stiffer equation of state of neutron-star matter and to reproduce maximum neutron star masses of $2M_{\odot}$, in agreement with recent astrophysical observations [2, 3]. This property is not achieved by the standard Gogny forces of the D1 family [4]. We also wanted to preserve the good description of finite nuclei at the Hartree-Fock-Bogoliubov (HFB) level provided by the D1M force [5]. In the fit of D1M* [1], we modified the eight finite-range strengths of the D1M force keeping the other parameters at their D1M values. Seven linear combinations of these strengths, related to different properties of symmetric nuclear matter, and the pairing strengths in the $S=0$, $T=1$ channel, were constrained to take the same values as in D1M. The eighth combination was used to modify the slope of the symmetry energy and, therefore, the prediction for the maximum neutron star mass. Finally, the t_3 parameter was fine tuned to obtain a finite nuclei description with similar quality to D1M for the same set of nuclei. All of the finite nuclei calculations in [1] were carried out with the

HFBaxial code [6] using an approximate second-order gradient method to solve the HFB equations in a harmonic oscillator (HO) basis including up to 19 major oscillator shells and the oscillator lengths adapted to the characteristic length-scale dependence with mass number. Notice that HFB calculations of deformed nuclei with Gogny interactions are usually performed in a HO basis since the seminal paper of Dechargé and Gogny [7].

In the recent manuscript 1806.02080v1 [8], it is found that this new D1M* Gogny force and the D1N force suffer from the existence of spurious finite-size instabilities in the $S=0$, $T=1$ channel. These instabilities are detected through a fully antisymmetrized RPA calculation of the nuclear matter response functions based on the continued fraction technique [9]. This procedure was applied in [9] to the search of instabilities in standard Gogny forces as well as forces of Gogny type including tensor terms. In this study, in agreement with the results of similar analyses carried out for Skyrme functionals [10], it was concluded that the key quantity to detect spurious finite-size instabilities is the critical density, which makes the nu-

cleus unstable if it reaches a value $\rho_c \simeq 0.20 \text{ fm}^{-3}$ for a momentum transfer of about 2.5 fm^{-1} . This critical density of $\rho_c \simeq 0.20 \text{ fm}^{-3}$ may be reached in HF calculations of some nuclei, as for example ^{40}Ca . The instabilities of D1M* and D1N were predicted in nuclear matter [8, 9] and their appearance in calculations of nuclei in coordinate space is verified in [8] by performing HFB calculations of finite nuclei on a mesh assuming spherical symmetry, using the Gogny forces with the FINRES₄ code [11]. From the results shown in [8], it can be seen that the neutron and proton density profiles are very delicate quantities, which are largely affected in the center of the nucleus by the finite-size instabilities, showing a continuously increasing or decreasing trend as a function of the number of iterations in the iterative solution of the non-linear HFB equation, without reaching a stabilized value. In another paper [10], a similar study was done in the framework of Skyrme forces.

In the present manuscript we provide additional information about the possible impact of the finite-size instability in the $S = 0, T = 1$ channel, detected in [8], on the binding energies, neutron and proton radii and density profiles of finite nuclei computed using the D1M* interaction with the HO basis [1]. The tests performed support the fact that the predictions for finite nuclei obtained with D1M* with the HO basis in [1] are robust. We also perform spherical HF calculations with D1M* on a mesh in coordinate space. In spite of the non-convergent behavior of the nucleon density profiles, there is an optimal number of iterations for which integrated quantities such as the total binding energies present a plateau pattern. When we compare the D1M* binding energies obtained with the HO basis and these values computed on a mesh, we observe an excellent agreement between both sets of results. The quality of this agreement in D1M* is equivalent to the one we find in the same type of comparison if we use D1M, which does not have finite-size instabilities.

In our finite-nuclei deformed calculations performed using the HO basis for over 600 even-even nuclei and covering the whole nuclear chart [1], we did not face any lack of convergence in the nucleon density profiles similar to the one discussed in [8]. The difference between the two calculations is our use of a HO basis instead of using a mesh as in Ref. [8]. It is well known that the HO basis introduces an ultraviolet cutoff, due to its Gaussian falloff in momentum space, which acts as a regulator for the behavior related to high-momentum components in the wave function. On the other

hand, mesh calculations are more prone to suffer the effect of possible ultraviolet divergences. This difference between HO basis and mesh calculations was already recognized in [8], where it was argued that the use of a HO basis “strongly renormalizes the interaction and inhibits the development of instabilities” and that “the D1M* interaction should only be used with the basis employed to fit its parameters”. From this statement one should expect significant changes in the value of physical observables computed with the D1M* force when the HO basis size is increased or its harmonic oscillator lengths modified. To test this statement, we have carried out calculations with different HO basis sizes including 11, 13, 15, 17, 19 and 20 full HO shells for some representative nuclei using both D1M* and D1M. Larger basis are impractical for Gogny calculations involving deformed nuclei and therefore are not currently implemented in the HFBaxial code. In all the cases analyzed, we observe a similar behavior of the observables as a function of the number of shells in both the D1M* and D1M cases. The range of nuclei considered includes deformed nuclei like ^{224}Ra , ^{168}Er or ^{48}Cr and spherical nuclei like ^{16}O , ^{40}Ca , ^{56}Ni , ^{100}Sn , ^{132}Sn or ^{208}Pb . Except for the binding energy (which is the variational magnitude and therefore always increases with increasing basis size), the changes in the other observables (radii, quadrupole deformation, octupole deformation, etc.) are less than one in a thousand when going from the smallest to the largest basis size. Interestingly, the convergence rate with basis size of the density at the origin is rather slow and requires a large number of shells both in D1M and D1M*, and even in the D1S case, as can be seen in Figs. 1–4, where the neutron and proton densities of ^{208}Pb computed with D1M and D1M* with different number of HO shells are displayed by solid lines. It is to be pointed out that the central density does not enter significantly in most of the observables like radii or multipole moments as the corresponding operators go to zero at the origin. Also the energy, which should be more sensitive through the strongly repulsive density-dependent part of the interaction to the slow converge rate of the central density, shows a smooth behavior. We also would like to mention that in Ref. [12] we studied fission properties of the uranium isotopes including very neutron-rich isotopes using the parametrizations D1S, D1M and D1N. From some of the claims of Ref. [8] questioning the fact that one usually uses different HO parameter values for different nuclei and shapes, one could

have expected to observe erratic results in the calculations with D1N, which may also show finite-size instabilities [8]. However this is not the case, in spite of using in the fission calculations, which require very large deformations, a HO basis (size and oscillator lengths) very different from the one used in the D1N fit, tailored to the ground state. This is an additional indication that the regularization of the ultraviolet sector of the force as a consequence of using a HO basis renders the predictions of D1N as reasonable as the ones of D1S and D1M.

In order to analyze more deeply the findings of Ref. [8] concerning finite nuclei calculations on a mesh with D1M*, we have performed HF calculations using the method described in [13], where the HF exchange energy is approximated by a quasiloca approach calculated using the extended Thomas-Fermi expansion of the density matrix derived in [14]. This approach is similar to the density matrix expansions proposed by Negele and Vautherin [15] or by Campi and Bouyssy [16]. The quasiloca approximation allows one to write the energy density functional for finite-range effective interactions in a local form and enables HF calculations in coordinate space in a similar fashion to the case of Skyrme forces [17]. This quasiloca approach, which is discussed in detail in [13], gives results that are very close to the full HF results calculated with HO basis as can be seen in Refs. [13, 18, 19]. The HF nucleon densities we obtain in a mesh with the quasiloca approximation nicely agree with the corresponding densities obtained using the FINRES₄ code [11], as can be seen from Figs. 1 and 2 for the ²⁰⁸Pb neutron and proton densities computed with the D1M interaction. From these figures we also see that the shell oscillations in the center of the nucleus of the densities obtained by the mesh calculation are more pronounced than the shell oscillations provided by the HO basis. This is a first qualitative indication that the mesh densities may be more affected by the finite-size instabilities than the densities calculated with a HO basis. We shall also point out that the quasiloca approach is very well suited for the analysis of instabilities in spherical nuclei in coordinate space, as it reproduces all the instabilities of finite nuclei reported in [8].

To test the consistency between the HO basis and mesh quasiloca calculations, we show in Table 1 the binding energies computed with the D1M force in a HO basis using the HFBaxial code for the magic nuclei ¹⁶O, ⁴⁰Ca, ⁵⁶Ni, ⁹⁰Zr (all of them with 15 HO shells), ¹³²Sn (with 17 HO shells) and

Table 1: Quantal D1M HF binding energies in doubly magic nuclei computed using the HO basis and the quasiloca approximation in coordinate space (mixing factor 0.9).

| Nucleus | $B_{\text{HO}}(\text{MeV})$ | $B_{\text{QLA}}(\text{MeV})$ |
|-------------------|-----------------------------|------------------------------|
| ¹⁶ O | 128.02 | 127.02 |
| ⁴⁰ Ca | 341.67 | 340.53 |
| ⁵⁶ Ni | 478.65 | 478.17 |
| ⁹⁰ Zr | 781.26 | 781.29 |
| ¹³² Sn | 1102.57 | 1103.31 |
| ²⁰⁸ Pb | 1636.08 | 1637.96 |

Table 2: Quantal D1M* HF binding energies in doubly magic nuclei computed using the HO basis and the quasiloca approximation in coordinate space with 100 and 150 iterations (mixing factor 0.9).

| Nucleus | $B_{\text{HO}}(\text{MeV})$ | $B_{\text{QLA}}^{100}(\text{MeV})$ | $B_{\text{QLA}}^{150}(\text{MeV})$ |
|-------------------|-----------------------------|------------------------------------|------------------------------------|
| ¹⁶ O | 128.32 | 127.29 | 127.29 |
| ⁴⁰ Ca | 342.55 | 341.33 | 341.35 |
| ⁵⁶ Ni | 481.34 | 479.41 | 479.41 |
| ⁹⁰ Zr | 783.14 | 782.58 | 782.60 |
| ¹³² Sn | 1103.08 | 1103.25 | 1103.82 |
| ²⁰⁸ Pb | 1636.73 | 1637.83 | 1638.18 |

²⁰⁸Pb (with 19 HO shells). The oscillator lengths have been optimized as to minimize the energy. In the same table we display the D1M binding energies from the spherical HF calculation on a mesh in coordinate space using the quasiloca approach, which are well converged as far as the D1M force is free from finite-size instabilities, in agreement with [8]. It can be seen that the results from the HF method in the HO basis and on a mesh are in excellent agreement among them. Notice that the two solutions cannot be identical because, besides the fact that the phase spaces and numerical methods of the two calculations are very different, the mesh calculation implements the quasiloca approximation of the exchange potential. In Table 2 we show the binding energies predicted by the D1M* force for the same nuclei computed with both the HO basis and the quasiloca approach in coordinate space after certain numbers of iterations. We can see that the D1M* HF quasiloca energies show a nearly stable behavior over a range of iterations. In this range the agreement between the D1M* binding energies computed in a HO basis and in a mesh is similar to that found using the D1M force. The binding energies reported in

Tables 1 and 2 show the consistency of the HFB results in a HO basis, which do not depend on details such as the size and oscillator lengths of the basis within the range of 20 oscillator shells. The impact of the finite-size instabilities in the D1M* calculations on a mesh is much more relevant in the neutron and proton density profiles around the center of the nucleus as can be seen in Figs. 3 and 4 for ^{208}Pb . The nucleon densities from the mesh calculation in the quasilocal approach with D1M* exhibit a divergent trend against the number of iterations, which does not happen when the densities are calculated with the D1M force. This situation with the HF densities in coordinate space is different from the one shown by the densities computed in a HO basis, where the central densities exhibit a convergent trend with the number of HO shells used in the calculation for both the D1M and D1M* forces.

Additional results of our numerical investigations for D1M* are collected in Figs. 5–21. We find that the D1M* HF results calculated with the quasilocal approximation show the same instabilities as the HFB mesh calculations of [8]. Our HF calculations of the nuclei ^{40}Ca and ^{208}Pb with D1M* show a non-convergent behavior as a function of the number of iterations as can be seen in Figs. 5–16. Again, as can be seen in Figs. 7 and 10 for ^{208}Pb and Figs. 13 and 16 for ^{40}Ca , the central densities are the most strongly affected quantities by the finite-size instabilities, increasing or decreasing their values with the number of iterations, in agreement with the results reported in [8]. The impact of the finite-size instabilities on the energies is shown in Figs. 5 and 8 for ^{208}Pb and Figs. 11 and 14 for ^{40}Ca . We note that as a function of the number of iterations the total energies show a plateau structure, before eventually diverging for a larger number of iterations. The number of iterations where the energy is nearly stable depends, of course, on the initialization conditions and the mixing factor. This factor combines some quantities obtained in a given iteration with the same quantities of the previous iteration in order to slow down and stabilize the iterative process. The results in Figs. 5–16 were obtained with a mixing factor of 0.9 starting from a Woods-Saxon (WS) shape for the initial mean-field potential. If the mixing factor is changed or the initial potential is changed (e.g., by using other WS parameters or the converged mean field of a calculation with D1M or D1S), basically the same results are reached in the plateau region (see Figs. 17 and 18), although the beginning and width of the plateau

may involve another number of iterations. An additional gauge of the convergence is provided by the stationarity condition arising from the scaling transformation $\mathbf{r} \rightarrow \lambda \mathbf{r}$ [20], which is equivalent to the virial theorem [21]. Notice that the stability against the scaling transformation is a very strict condition as it comes from the cancellation of quantities that individually are very large. We display in Figs. 8 and 14 the derivative of the scaled energy with respect to the scaling parameter at $\lambda = 1$, i.e., $dE(\lambda)/d\lambda|_{\lambda=1}$. We see that in a relatively large range of iterations, which coincides with the range where the energies are almost flat, $dE(\lambda)/d\lambda|_{\lambda=1}$ takes a rather constant value close to zero, pointing out the near stability of the energy within this number of iterations. We have also checked the impact of the instabilities on other quantities directly related to the nucleon densities such as the neutron and proton rms radii. We display the rms radii in Figs. 6 and 9 (Figs. 12 and 15) for ^{208}Pb (^{40}Ca). We see that the impact of the instability is relatively more important in ^{208}Pb than in ^{40}Ca , although these radii can be estimated with less than 0.5% variation in the range of iterations where the energy is quasi stable.

Further information about the D1M* HF calculations in coordinate space can be extracted from Figs. 19–21 displaying the energy per particle and the neutron and proton central densities of the nuclei ^{16}O , ^{22}O , ^{40}Ca , ^{56}Ni , ^{100}Sn and ^{176}Sn as functions of the number of iterations (mixing factor 0.9 in these calculations). From these figures we see that ^{40}Ca becomes unstable rather quickly, the energy of ^{56}Ni is stable until around 1700 iterations, and ^{16}O , ^{22}O , ^{100}Sn and ^{176}Sn are stable (we ran up to 10000 iterations). These results and the shell structure of these nuclei suggest that the appearance of instabilities in coordinate space is directly related with the existence of s -orbitals close to the Fermi level. As pointed out in [8], and confirmed also in our calculations, the ^4He nucleus is unstable with D1M* on a mesh. Both this nucleus and ^{40}Ca have an s -orbital in the last occupied shell and very close to the Fermi level. In the case of ^{56}Ni the energy gap between the $2s_{1/2}$ level and the Fermi level (~ 7 MeV) is larger than in ^{40}Ca (~ 1.5 MeV) but smaller than in the ^{16}O nucleus (~ 20 MeV) and the ^{100}Sn nucleus (~ 16 MeV) that are stable. In the case of ^{176}Sn , in the proton spectrum the $2s_{1/2}$ level remains at ~ 12 MeV from the Fermi level, and in the neutron spectrum the $3s_{1/2}$ level is also deep, at ~ 10 MeV from the last occupied orbit.

Our findings are in harmony with the claim of

Ref. [8] that instabilities appear in HF calculations in coordinate space for densities larger than about 0.20 fm^{-3} as it happens in the paradigmatic nucleus ^{40}Ca . However, the same ^{40}Ca nucleus computed without Coulomb, in spite of having a similar value of the central density as the charged ^{40}Ca , is stable in the D1M* mesh calculation, as pointed out in [8] and confirmed in our quasilocal approach. Hence, some neutron-proton asymmetry is needed to trigger the instability in the calculations in coordinate space when s -orbitals close to the Fermi level are occupied. The role of the s -orbitals of the nucleus on the instabilities in a mesh seems to be further supported by the case of the ^{22}O and ^{24}O isotopes. We find in our HF mesh quasilocal calculations that ^{22}O is stable (the $2s_{1/2}$ neutron orbital is empty) and ^{24}O is unstable (the $2s_{1/2}$ neutron orbital becomes the Fermi level).

In the conclusions of Ref. [8] it was argued that beyond mean-field calculations with the D1M* interaction may be unsuitable. Although this may concern RPA calculations, to test the performance of D1M* in a beyond mean-field scenario, we have carried out Generator-Coordinate-Method (GCM) calculations with D1M* and D1M using the octupole moment as collective coordinate for neutron-rich Ra and Th isotopes. Again the D1M* and D1M results are very similar and only show some deviations for shape-coexistent nuclei or those with very soft potential energy surfaces where tiny changes in the interaction can lead to some noticeable changes in the observables. As an example of the results, we present in Fig. 22 the plot of the excitation energies of the 3^- states obtained in the GCM calculation for both D1M* and D1M. A perfect agreement between the two forces will lead to all the points sitting on top of the straight line. In the plot we observe small deviations for most of the 64 nuclei analyzed, and, in those cases where the deviations are not negligible, we have checked they correspond to nuclei with shallow minima where little details are more relevant.

From the discussions above we can conclude that:

- We are able to reproduce the results of [8] in coordinate space calculations on a mesh using the HF method applied to a quasilocal reduction of the energy density functional associated to the Gogny forces.
- In the mesh calculation the density at the origin is the most sensitive quantity to the finite size instability. Other quantities, like

the binding energy, radii or the virial theorem reach a broad plateau with very reasonable values (as compared to stable parametrizations) but those quantities eventually develop an instability if a sufficiently large number of iterations is used.

- The instabilities seem to be nucleus dependent and are apparently connected with the relative position of the last occupied s -orbital with respect to the Fermi level.
- The HO basis, with its natural ultraviolet cut-off, serves as a regulator of the finite size instabilities and in all the calculations carried out so far in a large variety of situations no instability is found. The results are always comparable to the ones of stable parametrizations.
- The conclusions of [8] regarding the unsuitability of the HO basis for finite nuclei calculations seem to us a bit far-fetched. Although in the limit of infinite HO shells the instabilities may be present, in the standard framework with Gogny forces where 20 harmonic oscillator shells are used at most, the convergence of most of the quantities with basis size is very good and there is not a spurious dependence with oscillator lengths.
- Finally, we find that D1M* is suitable for beyond mean-field calculations such as the GCM calculations discussed before.

We are now in the process of writing a paper showing the predictions of D1M* for a large set of finite nuclei observables and comparing them with the ones of D1M. We observe a very good agreement between the predictions of the D1M and D1M* parametrizations for finite nuclei (as it should be, given the guiding principles in the fit of D1M*, see [1]), in all the quantities analyzed, which include moments of inertia, spectra of odd nuclei, potential energy surfaces as a function of quadrupole and/or octupole multipole parameters, (β, γ) planes as required by the 5DCH, and even fission barriers in the actinides and the super-heavies. All these calculations have been carried out using a HO basis with a size as large as possible. We are confident on the regularization properties of the HO basis to yield good results in finite nuclei both at the mean-field and beyond mean-field levels even in cases where finite-size instabilities may appear in HF calculations on a mesh.

References

- [1] C. Gonzalez-Boquera, M. Centelles, X. Viñas and L.M. Robledo, *Phys. Lett.* **B779** (2018) 195.
- [2] P.B. Demorest et al., *Nature* **467** (2010) 1081.
- [3] J. Antoniadis et al., *Science* **340** (2013) 448.
- [4] C. Gonzalez-Boquera, M. Centelles, X. Viñas and A. Rios, *Phys. Rev.* **C96** (2017) 065806.
- [5] S. Goriely, S. Hilaire, M. Girod, and S. Péru, *Phys. Rev. Lett.* **102** (2009) 242501.
- [6] L.M. Robledo, HFBaxial computer code (2002).
- [7] J. Dechargé and D. Gogny, *Phys. Rev.* **C21** (1980) 1568.
- [8] M. Martini, A. De Pace and K. Bennaceur, arXiv:1806.02080v1 (2018).
- [9] A. De Pace and M. Martini, *Phys. Rev.* **C94** (2016) 024342.
- [10] V. Hellemans, A. Pastore, T. Duguet, K. Bennaceur, D. Davesne, J. Meyer, M. Bender and P.-H. Heenen, *Phys. Rev.* **C88** (2013) 064323.
- [11] K. Bennaceur, FINRES₄, (2018) unpublished.
- [12] R. Rodriguez-Guzman and L.M. Robledo, *Phys. Rev.* **C89** (2014) 054310.
- [13] V.B. Soubbotin, V.I. Tselyaev and X. Viñas, *Phys. Rev.* **C67** (2003) 014324.
- [14] V.B. Soubbotin and X. Viñas, *Nucl. Phys.* **A665** (2000) 291.
- [15] J.W. Negele and D. Vautherin, *Phys. Rev.* **C5** (1972) 1472.
- [16] X. Campi and A. Bouyssy, *Phys. Lett.* **B73** (1978) 273.
- [17] D. Vautherin and D.M. Brink, *Phys. Rev.* **C5** (1972) 626.
- [18] S. Krewald, V.B. Soubbotin, V.I. Tselyaev and X. Viñas, *Phys. Rev.* **C74** (2006) 064310.
- [19] B. Behera, X. Viñas, T.R. Routray, L.M. Robledo, M. Centelles and S.P. Pattnaik, *J. Phys.* **G43** (2016) 045115.
- [20] O. Bohigas, A.M. Lane and J. Martorell, *Phys. Rep.* **51** (1979) 267.
- [21] E. Merzbacher, *Quantum Mechanics*, Wiley & Sons 1961, p.168.

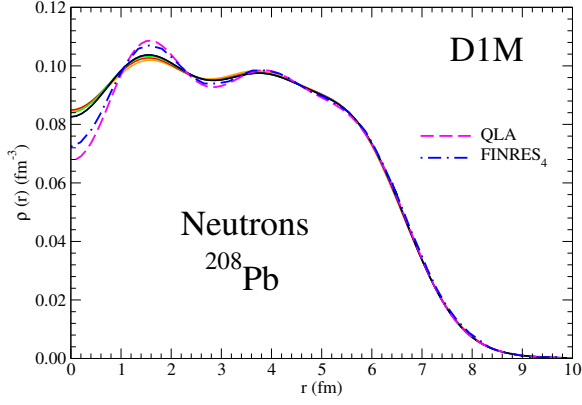


Figure 1: Solid lines: Neutron density of ^{208}Pb computed with the D1M force with a HO basis with 12, 14, 16, 18 and 19 shells. Dashed lines: The same density obtained through a HF calculation on a mesh in the quasilocal approach. Dash-dotted lines: The same density extracted from Fig. 3 in Ref. [8].

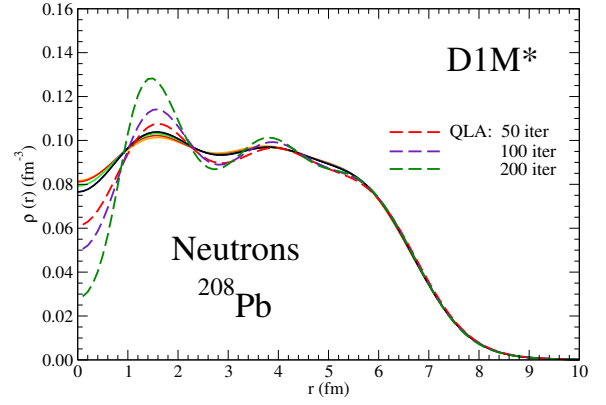


Figure 3: The same as in Fig. 1 but computed with the D1M* force. The HF density is displayed for three different number of iterations.

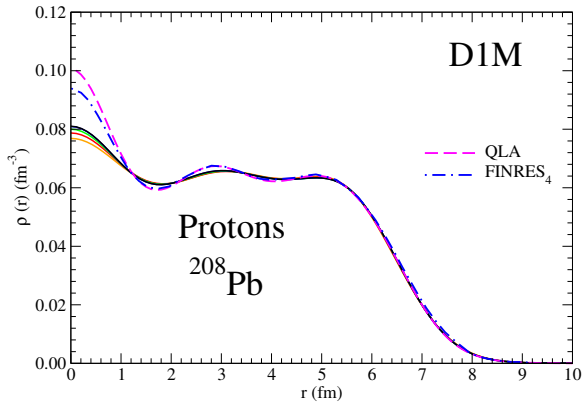


Figure 2: The same as in Fig. 1 but for the proton density.

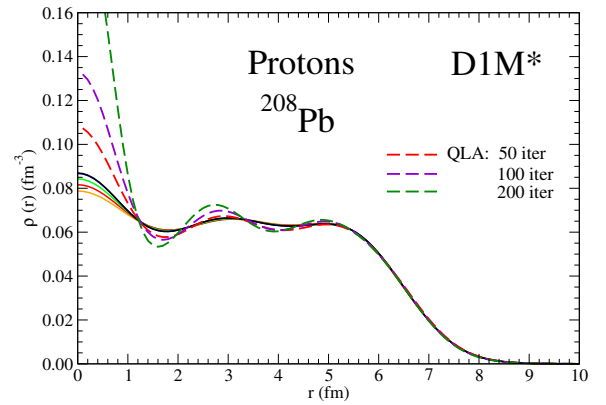


Figure 4: The same as in Fig. 3 but for the proton density.

^{208}Pb

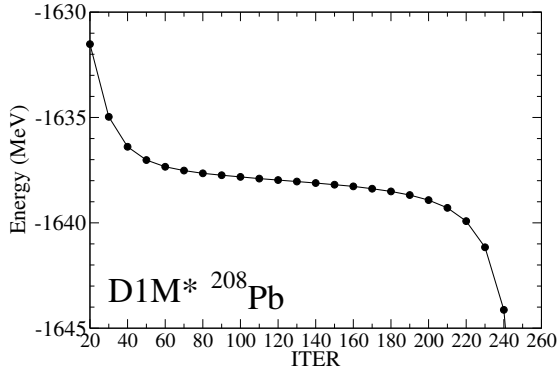


Figure 5: Total energy against the number of iterations of the calculation on a mesh, for ^{208}Pb with the D1M* interaction.

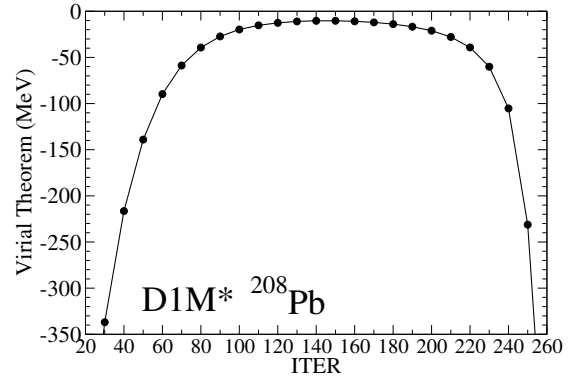


Figure 8: Virial theorem against the number of iterations of the calculation on a mesh, for ^{208}Pb with the D1M* interaction.

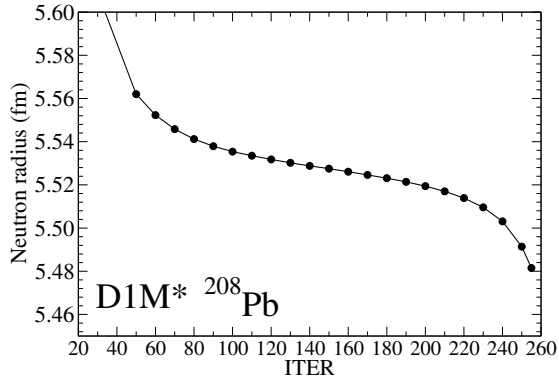


Figure 6: Neutron radius against the number of iterations of the calculation on a mesh, for ^{208}Pb with the D1M* interaction.

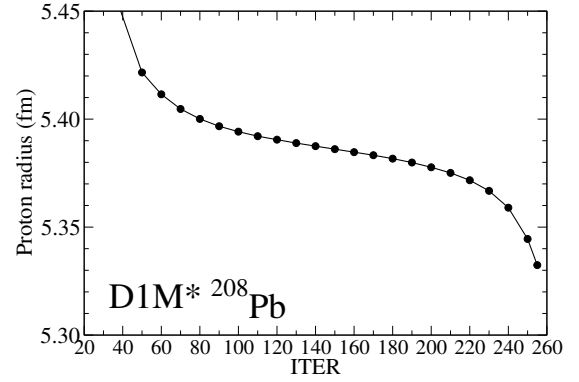


Figure 9: Proton radius against the number of iterations of the calculation on a mesh, for ^{208}Pb with the D1M* interaction.

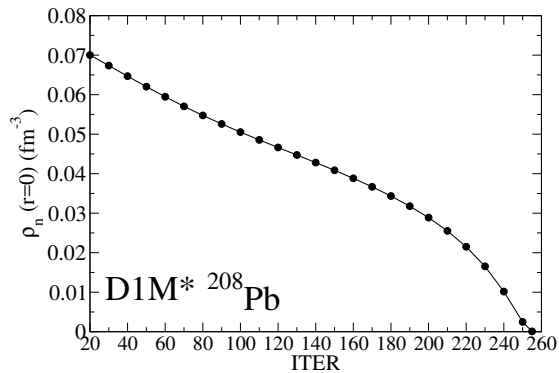


Figure 7: Neutron density at the origin against the number of iterations of the calculation on a mesh, for ^{208}Pb with the D1M* interaction.

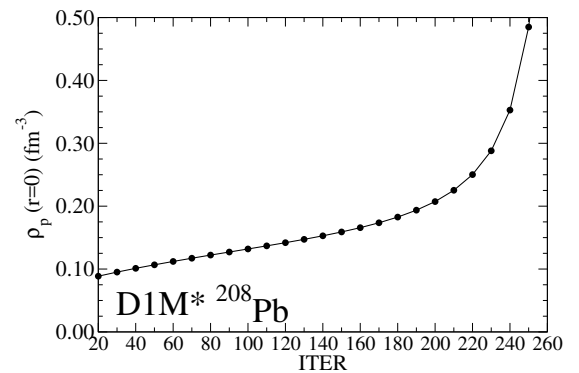


Figure 10: Proton density at the origin against the number of iterations of the calculation on a mesh, for ^{208}Pb with the D1M* interaction.

^{40}Ca

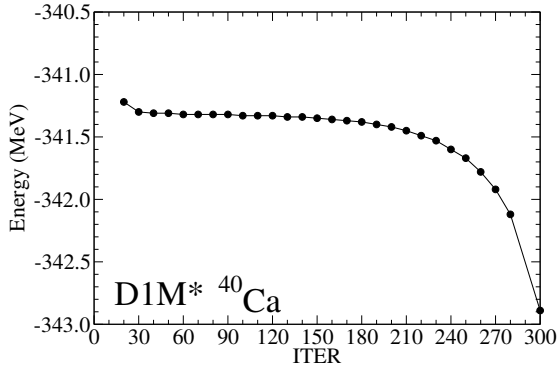


Figure 11: Total energy against the number of iterations of the calculation on a mesh, for ^{40}Ca with the D1M* interaction.

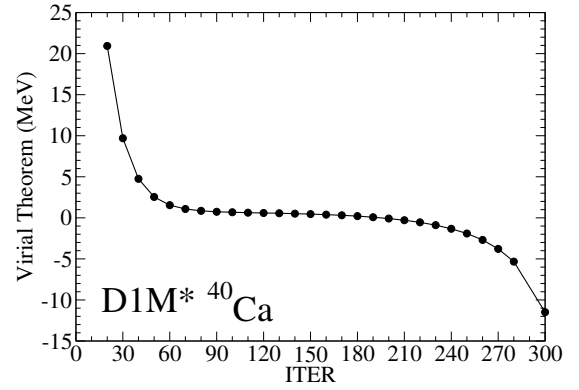


Figure 14: Virial theorem against the number of iterations of the calculation on a mesh, for ^{40}Ca with the D1M* interaction.

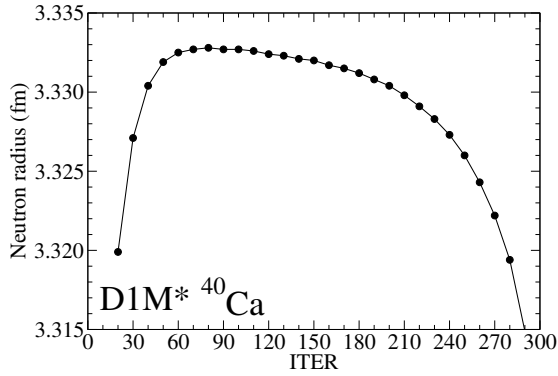


Figure 12: Neutron radius against the number of iterations of the calculation on a mesh, for ^{40}Ca with the D1M* interaction.

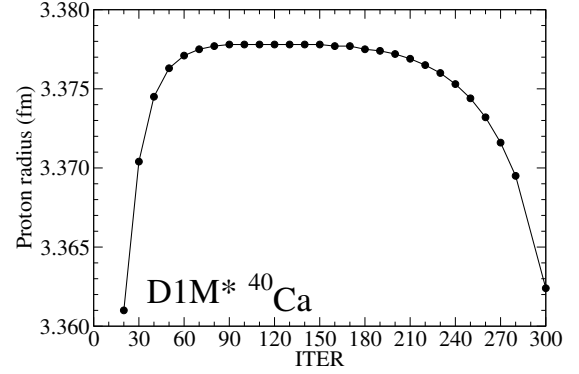


Figure 15: Proton radius against the number of iterations of the calculation on a mesh, for ^{40}Ca with the D1M* interaction.

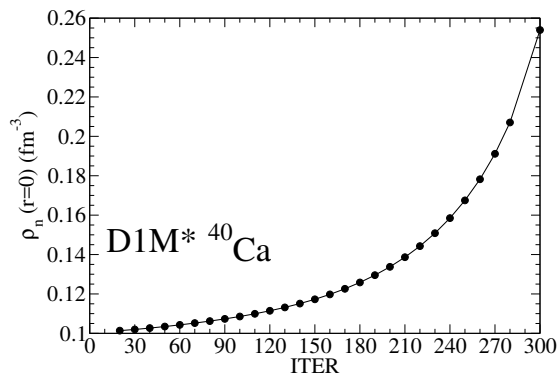


Figure 13: Neutron density at the origin against the number of iterations of the calculation on a mesh, for ^{40}Ca with the D1M* interaction.

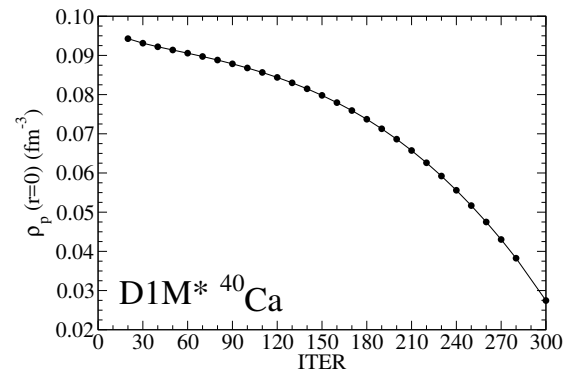


Figure 16: Proton density at the origin against the number of iterations of the calculation on a mesh, for ^{40}Ca with the D1M* interaction.

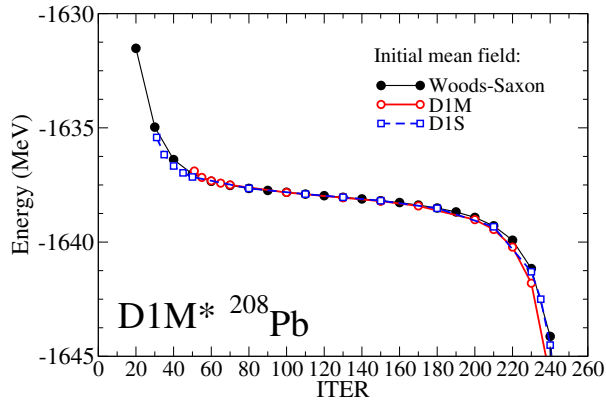


Figure 17: Energy against number of iterations of the calculation on a mesh for ^{208}Pb with D1M*. The calculation was started from a WS potential in the black curve (same curve of Fig. 5) and from the mean field of a converged calculation with the D1M or D1S interactions in the red and blue curves, respectively. The number of iterations on the abscissae corresponds to the case started from a WS potential; the other curves are shifted a few iterations to the right to visualize the coincidence of the results in the plateau region.

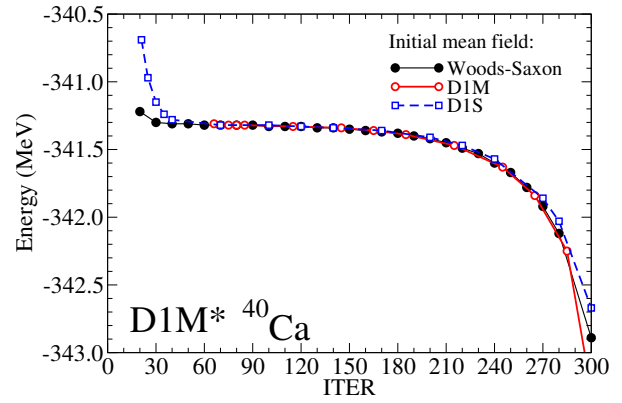


Figure 18: The same as in Fig. 17 but for ^{40}Ca .

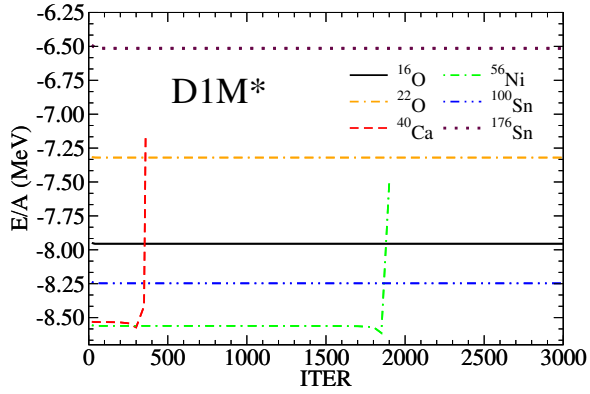


Figure 19: Energy per particle against the number of iterations of the calculation on a mesh, for the ^{16}O , ^{22}O , ^{40}Ca , ^{56}Ni , ^{100}Sn and ^{176}Sn nuclei with the D1M* interaction.

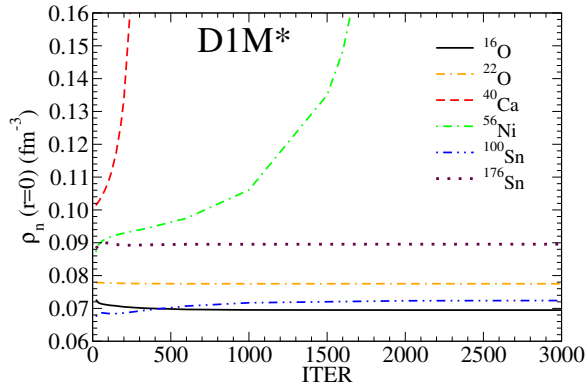


Figure 20: The same as in Fig. 19 but for the neutron density at the origin.

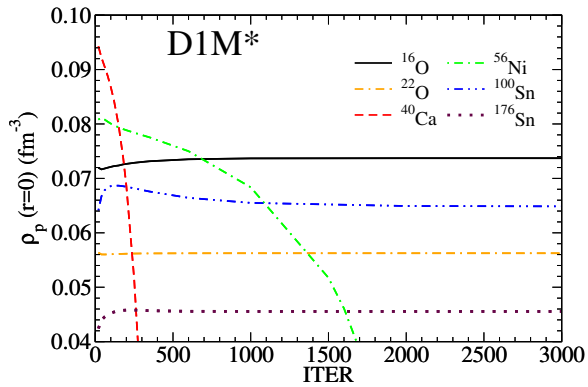


Figure 21: The same as in Fig. 19 but for the proton density at the origin.

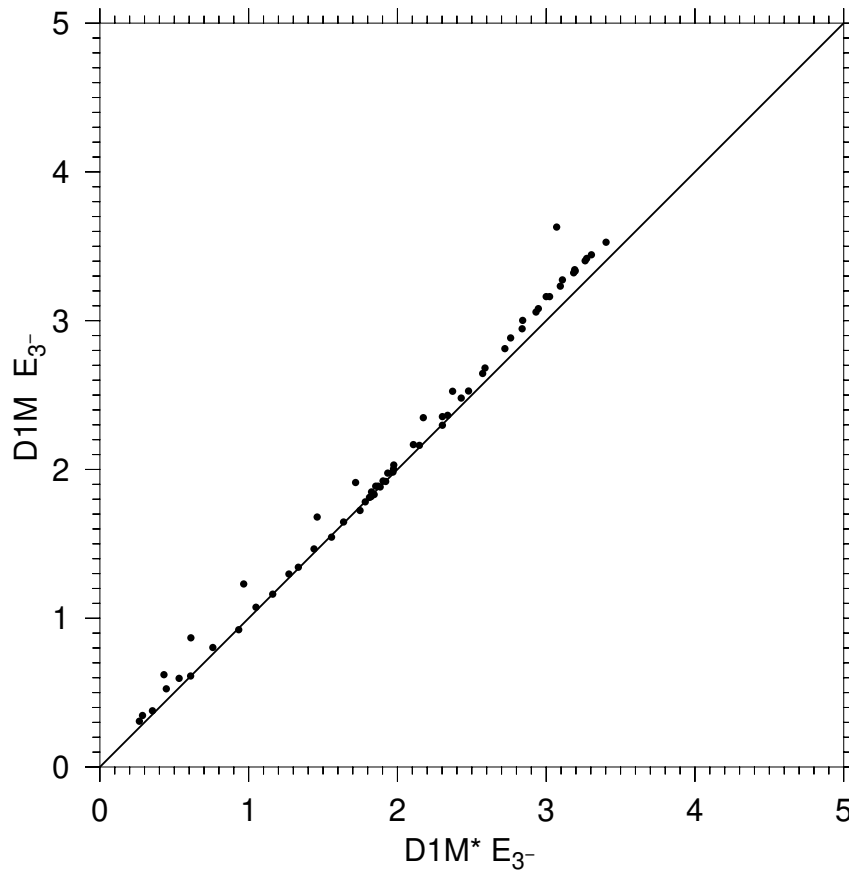


Figure 22: Comparison between the excitation energy of the 3^- state obtained in a GCM calculation using the octupole degree of freedom as collective coordinate for both D1M and D1M*.